Al-Nahrain Journal for Engineering Sciences **NJES** 27(2)199-206, 2024
http://doi.org/10.29194/NJES.27020199

All-Optical Switch Based on Thermo-Optic Effect in Graphene-on-Si_3N_4 Structure

Hayder Maki Hamodi[1], Raad Sami Fyath[2*]

Authors affiliations:
1) CERT Iraq, PMO, Iraq
hayderhamodi@gmail.com
2*) Department of Computer Engineering, College of Engineering, Al-Nahrain University, Iraq
rsfyath@yahoo.com

Paper History:
Received: 6th Apr. 2024
Revised: 6th Apr. 2024
Accepted: 16th June 2024

Abstract

A high-performance Mach-Zehnder interferometer (MZI) based all-optical switch using graphene on silicon nitride (Si_3N_4) is proposed and simulated. Graphene absorbs pump power (λ = 980 nm) on Si_3N_4 waveguide, generating heat. The heat affects the Si_3N_4 waveguide, causing a change in its refractive index due to thermo-optic effect. By tuning the probe phase (λ = 1550 nm) in the Si_3N_4 arm with graphene on top, all optical switching can then be carried out. An extinction ratio ranges of 13-25 dB and pump power range 20-270 mW. These findings demonstrate that our suggested configuration offers a useful integrated part for the creation of effective all-optical control devices on the insulator platform with a quick switching rate. Moreover, the suggested design might be able to achieve a wide bandwidth by utilizing an integrated MZI structure.

Keywords: Graphene Layer, Thermo-Optic, All Optical Switch.

مفتاح ضوئي بالكامل بناءًا على التأثير الحراري-الضوئي في مركب الكرافين-على-نتريد السيليكون

حيدر مكي حمودي , رعد سامي فياض

الخلاصة:

يتم اقتراح ومحاكاة مفتاح ضوئي بالكامل باستخدام تداخل ماخ-زندر (MZI) عالي الأداء بناءًا على الغرافين على نتريد السيليكون (Si_3N_4). يمتص الغرافين قدرة الضخ (λ = 980nm) على الدليل الموجي Si_3N_4، مما يولد حرارة. تؤثر الحرارة على الدليل الموجي Si_3N_4، مما يتسبب في تغيير معامل الانكسار الخاص به نتيجة لتأثير الحرارة البصرية. يمكن بعد ذلك تنفيذ جميع عمليات التبديل البصري من خلال ضبط مرحلة الاختبار (λ = 1550 nm) في ذراع Si_3N_4 مع الغرافين في الأعلى. نسبة الانقراض تتراوح بين(13-25 dB) ونطاق قدرة الضخ يتراوح بين (20-270 mW). توضح هذه النتائج أن التكوين المقترح يقدم جزء متكامل مفيد لإنشاء أجهزة التحكم البصرية كليًا الفعالة على منصة العازل بمعدل تبديل سريع. علاوة على ذلك، قد يكون التصميم المقترح قادراً على تحقيق عرض نطاق ترددي واسع من خلال استخدام هيكل MZI متكامل.

1. Introduction

All-optical switches are essential parts of all-optical signal processing, in order to avoid optical-electrical-optical (OEO) conversion and potentially create a power-efficient photonic system [1]. Efficient control of all-optical light has been followed through the exploration of fiber-based all-optical switches in recent times to get efficient control [2, 3]. In order to create a large-scale photonic system, it is highly desirable to have on-chip integration. Integrated all-optical switches have been successfully developed on semiconductor platforms such as silicon [4]. But, because this semiconductor has small bandgaps, it shows two-photon absorption (TPA) and free-carrier absorption (FCA) effects at telecommunication wavelengths, which cause it to use a lot of power and yield high losses in transmission [5, 6]. Among all low loss materials, silicon nitride (Si_3N_4), as an insulator material with a large bandgap, offers new opportunities to eliminate the TPA and FCA losses for integrated all-optical switches [7]. This material is also compatible with CMOS methods, has good production tolerance because of the low difference in refractive index, and has less transmission loss than silicon [4, 8]. Thus, Si_3N_4 platform may accomplish straightforward manufacturing techniques and little nonlinear losses through weak thermo-optic effect, as evidenced by the material's lower thermal conductivity (30 $W.m^{-1}.K^{-1}$) and thermo-optic coefficient (2.5×10^{-5} K) values compared to silicon (130 $W.m^{-1}$.

NJES is an **open access Journal** with **ISSN 2521-9154** and **eISSN 2521-9162**

K^{-1} and 1.8×10^{-4} K^{-1}). The poor thermo-optic effect of Si_3N_4 would hence increase power consumption and result in a low tuning efficiency for the thermo-optic tuning-based all-optical switching. Therefore, a novel mechanism is highly desired to realize effective all-optical switching based on Si_3N_4 and the thermo-optic effect [1, 9]. Graphene is a 2D material with many different electrical, visual, physical, and chemical properties. It has been studied in depth in different areas of optoelectronics, such as optical modulators and waveguides. Because of its photo-thermal properties, graphene is also a good choice for all-optical devices [10, 11]. Based on this information, graphene was suggested as a good option for using ohmic heating to get a thermo-optic effect. As an example, Gan et al. reported in 2015 that when 980 nm is used to pump a graphene phase shifter in a Mach-Zehnder interferometer (MZI), one can get a nearly linear slope of 0.091 mW^{-1} [8, 12].

In this work, an all-optical switch uses graphene and Si_3N_4 on silica (SiO_2) and based on an MZI configuration is suggested and investigated to increase tuning efficiency. The signal and pump wavelength are 1550 and 980 nm, respectively. The device is simulated by COMSOL Multiphysics, ver. 6.1.

2. Device Structure and Operational Principles

The suggested MZI all-optical switch based on a graphene structure is implemented on silicon substrate as depicted in Fig. 1(a). The graphene is buried underneath SiO_2 clad and covers the upper core arm of the MZI rectangular waveguide which is made by Si_3N_4 material. Two Y-couplers and one directional coupler are used to implement the suggested device, along with two identical and equal length waveguide arms. Si_3N_4 (core)/ SiO_2 (cladding)/Si (substrate) waveguides are used with the dimensional parameters (height and width) of (h_{co}, w_{co}) and (h_{cl}, w_{cl}) for core and cladding, respectively, and the substrate is from Si, as shown in Fig. 1(b). As seen in Fig. 1(c), launches the input optical signal into the two arms of the MZI, and DC collects it at the output end. At the end of MZI, the optical signal is split to the two output ports (Port3 and Port4) with splitting ratio controlled by the pump power. A graphene layer completely covers the top waveguide arm. The input optical signal (probe) and the pump are applied at the input ports (Port1 and Port2), respectively. According to estimates, graphene causes a propagation loss of 4.6 dB, which means that the graphene layer absorbs 66% of the top arm's pump power [1, 13]. It is necessary to pump more optical power to the upper arm in order to make use of the absorption caused by the graphene.

Using Y-coupler with 50:50 splitting ratio ensures high-extinction ratio for the designed switch. The suggested device operates on the principle of utilizing the thermo-optic effect induced by graphene. By injecting the pump and probe light into the device, the graphene layer on top of the Si_3N_4 upper arm waveguide absorbs the pump light. Due to graphene's excellent thermal conductivity (5000 $W.m^{-1}.K^{-1}$) and very effective light absorption, heat created locally may be swiftly spread over the whole graphene region [12, 14], The generating heat is then increasing the temperature in the upper arm of the waveguide. The thermal conductivities of three materials, SiO_2, Si_3N_4, and graphene, are 1.38, 29, and 2000 $W\cdot m^{-1}.K^{-1}$, respectively [1, 15]. This allows for spreading the heat in core faster than cladding and this thermal tuning of core refractive index results in a change in phase shift for the probe light. Optical switching is achieved when a π-phase shift is obtained between the signal components in the two arms [16].

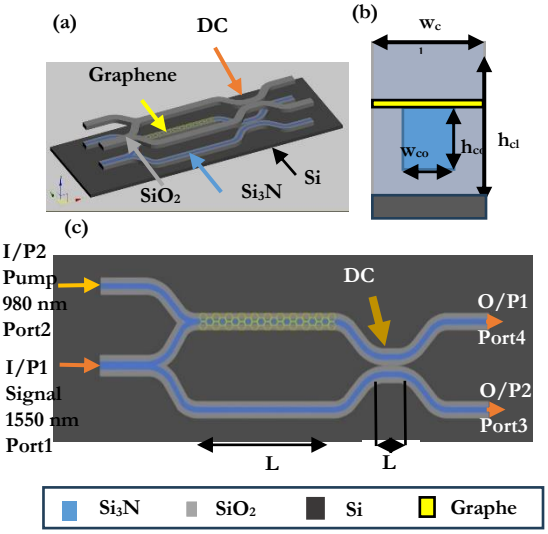

Figure (1): (a) 3D schematic diagram of the designed all-optical switch. (b) Sectional view of the graphene coating the MZI upper arm. (c) top view of MZI.

In order to assess the switching capability of suggested switch, one should initially examine the correlation between the injected pump power P_p and the resulting temperature variation ΔT in the Si_3N_4 waveguide. Thermo-optic switching is achieved due to graphene absorption. The graphene effective permittivity ε_g (= ng2). When there is only one layer of graphene, it is possible to calculate the electronic relaxation time, optical angular frequency, and Fermi level of graphene. Additionally, the Kubo formalism can be used to calculate the intraband and interband conductivity of graphene

$$\sigma = \sigma_{intra} + \sigma_{inter} \quad \ldots(1)$$

The dielectric constant of vacuum, denoted as ε0, the angular frequency ω, and the artificial thickness of graphene L_{eff} = 0.5 nm are all factors in Equation (1). As long as the formula for σ is known, this equation can be applied directly in standard full-wave simulations [17].

$$\sigma_g(\omega) = \frac{ie^2}{\pi\hbar}\frac{k_BT}{\hbar(\omega+i\Gamma^{-1})}\left[\frac{E_F}{k_BT} + 2\ln\left(e^{-\frac{E_F}{k_BT}} + 1\right)\right] + \frac{e^2}{4\pi}\left[\theta(\hbar\omega - 2E_F + \frac{i}{\pi}\ln\left|\frac{\hbar\omega-2E_F}{\hbar\omega+2E_F}\right|\right] \quad \ldots(2)$$

The first and second terms refer to the single-particle transitions within and between bands,

respectively. In this equation, $\hbar$ is reduced Planck's constant, kB is Boltzmann constant, and T is the temperature, e is electron charge, ln(x) is natural logarithm, and Θ(x) is Heaviside function. The dominant damping factor in plasmonic systems, known as the relaxation time Γ, is defined as Γ = μEF/(evF2), where the Fermi velocity vF = 106 m/s. Graphene allows for tuning of the Fermi level EF and carrier mobility μ to create plasmonic resonances as needed, with fixed values of EF = 0.6 eV and μ = 10000 cm2/(Vs) unless otherwise specified. Graphene is a good heat source because it has a high thermal conductivity. To keep things simple, the linear temperature distribution of the Si_3N_4 waveguide could be ignored. Instead, the 2D graphene-on- Si_3N_4 structure could be used to study the transverse temperature distribution. Then, it is assumed that the heat produced by graphene is the same all over the surface of the Si_3N_4 waveguide, leading to heat density in the graphene layer Q. As result, changing in refractive index with temperature can be calculated by

$$n(T) = n_0(n_0) + \frac{dn}{dT}\Delta T = \Delta n \quad \ldots(3)$$

where ∂n/∂T is the thermo-optic coefficient. With continuous pumping, the temperature distribution in the waveguide T is described by the steady-state heat conduction equation [18].

$$Q = -\kappa \nabla^2 T \quad \ldots(4)$$

where κ is the thermal conductivity of the material, ∇^2 is the Laplacian operator ($\nabla^2 = \frac{\partial^2}{\partial x^2} + \frac{\partial^2}{\partial y^2} + \frac{\partial^2}{\partial z^2}$ ... where x, y and z are the system coordinates) and Q is the generated heat density can be calculated by [1]

$$Q = \frac{P_p K_p \alpha_g}{w_g h_g l_g} \quad \ldots(5)$$

where Kp is the coupling ratio of the pump power to the upper waveguide, α_g is the graphene absorption ratio of optical pump power. Corresponding to this value of Q there is a change in temperature of Si_3N_4 core, it produces a change in the refractive index, thus, resulting in phase change as given by

$$\Delta\varphi = \frac{2\pi}{\lambda}\Delta n l = \frac{2\pi}{\lambda} l n_2 I \quad \ldots(6)$$

The DC is made up of two waveguides that are close to each other as explained in Fig. 2. When the distance between the two waveguides is small enough to allow evanescent contact, the light from one of the waveguides flows into the other. In the case of two identical waveguides, all the light power sent into one waveguide is sent to the other after travelling a distance called the coupling length L_c. This length can be calculated as

$$L_c = \frac{\pi}{2\gamma} \quad \ldots(7)$$

where $\gamma^2 = \kappa_c^2 + \Delta_m^2$, kc is the coupling coefficient, and Δm is the mismatch between the two super modes. At 50% power transfer, the 3dB coupling length of the DC is given by [19]

$$L_{3dB} = \frac{L_c}{2} \quad \ldots(8)$$

As illustrated in Fig. 1(c), the constructed 1×2 MZI consists of three main parts; the 1st part is Y-coupler which splits the input signal into two parts for each arm of MZI (the 2nd part of MZI), and the last part is DC, additionally, the 2nd Y-coupler is to guarantee that the injection pump power goes to the upper arm. The arm's length or the refractive index must be different to make a phase difference; in this case, the designed MZI has identical arm lengths.

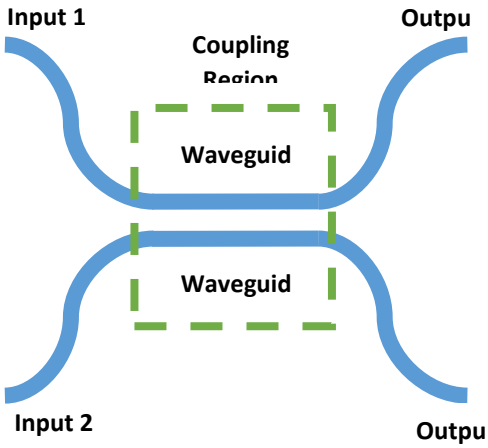

Figure (2): Schematic diagram of the directional coupler.

The 3rd part is the DC which combines the signal of both arms. Two EM waves interferes with each other constructively or destructively depending on the phase difference. The light can be split into two guided waves or combine into one wave when the branch is used reversely. For plane wave, the electric field is subjected to either constructive or destructive interference depending on weather the two arms have the same phase or a π phase difference, respectively.

The output of the MZI rests on the splitting ratio of the couplers and the losses in the two arms of the MZI. For lossless MZI configuration designed with 3dB couplers, Eqs.9 (a) and (b) show the relationship between output power Pout and input power Pin for the bar and cross states of operation, respectively [19]

$$\frac{P_{out1}}{P_{in}} = \sin^2\left(\Delta\beta \frac{L_w}{2}\right) \quad \text{(bar)} \quad \ldots(9\ a)$$

$$\frac{P_{out2}}{P_{in}} = \cos^2\left(\Delta\beta \frac{L_w}{2}\right) \quad \text{(cross)} \quad \ldots(9\ b)$$

where $\beta = \frac{2\pi}{\lambda} n_{eff}$ is propagation constant which is affected by changing in refractive index, $neff$ is the effective index of the upper arm waveguide. Lw is the arm length which is equal to the graphene layer length lg in the suggested device. Equation 9 (a) and (b) are assume that the input signal of power Pin is

applied at Port1, and the output powers, Pout1 and Pout2 are taken from Port3 and Port4, respectively (see Fig.1 (c)). Note that the phase shift between the two arms $\Delta\varphi = \Delta\beta\ L_w/2 = 2\pi\Delta n\ L_w/\lambda$. When $\Delta\varphi = m\pi$ with m = 0 or even integer, the Pout1/Pin = 0 and Pout2/Pin =1, thus, the input signal applied at Port1 will completely be directed to Port4. In contrast the signal will be directed to Port3 when $\Delta\varphi = m\pi$ with m is an odd integer number.

Graphene can be used as a heater to build the phase changer in Si_3N_4 waveguides by using the thermo-optic effect. By making the difference in phase between the two arms 0 or π, one can switch the output from the bar state to the cross state and back again. The thermal power generated by the graphene layer can be deduced from Eq. 5 as

$$P_{tg} = K_p \alpha_g P_p \qquad \ldots(10)$$

Part of this generated thermal power will transfer to the underneath waveguide leading to a change in its thermal power P_{tw}

$$\Delta P_{tw} = \frac{K_{th}}{L_w}\ K_p\ \alpha_g P_{tg} \qquad \ldots(11\ a)$$

where K_{th} is the thermal coupling parameter between graphene layer and the waveguide which is structure and material dependent and P_{tw} is the effective thermal power of the waveguide. The parameter ΔP_{tw} can be expressed as

$$\Delta P_{tw} = \frac{1}{L_w}[\sigma_{co}A_{co} + \sigma_{cl}A_{cl}\ ]\ \Delta T \qquad \ldots(11\ b)$$

where ΔT is the change in waveguide temperature. Further, the core (cladding) of the waveguide is characterized by $\sigma_{co}(\sigma_{cl})$ thermal conductivity and $A_{co}(A_{cl})$ area.

Using Eqs. 10 and 11 (a) into Eq. 11 (b) yields

$$\Delta T = \frac{K_{th}K_p\alpha_g P_p}{K_{\sigma A}} \qquad \ldots(12\ a)$$

where

$$K_{\sigma A} = \sigma_{co}A_{co} + \sigma_{cl}A_{cl} \qquad \ldots(12\ b)$$

From Eq. (12 a), the optical-to-thermal conversion coefficient COTC is given by

$$\text{COTC} = \frac{\partial T}{\partial P_p} = \frac{K_{th}K_p\alpha_g}{K_{\sigma A}} \qquad \ldots(12\ c)$$

The optic-optic coefficient (OOC) $\partial n_{eff}/\partial P_p$ can be estimated as the product of thermo-optic coefficient (TOC) $\partial n_{eff}/\partial T$ and optical-to-thermal conversion coefficient COTC

$$\partial n_{eff}/\partial P_p = \partial n_{eff}/\partial T\ .\ \partial T/\partial P_p \qquad \ldots(13\ a)$$

To get $\Delta\varphi\ (= \Delta\beta \mathrm{Lw}/2\ ) = \pi$, one should tune the effective refractive index to $(\Delta n_{eff})_\pi = \lambda/2\mathrm{Lw}$ This requires thermal tuning to yield

$$(\Delta T)_\pi = \frac{(\Delta n_{eff})_\pi}{\partial n_{eff}/\partial T} = \left(\frac{\lambda}{2L_w}\right)\frac{1}{\partial n_{eff}/\partial T} \qquad \ldots(13\ b)$$

In order to calculate the required power to get π-phase shift Eq. 12 a can be expressed as

$$(P_p)_\pi = \frac{K_{\sigma A}\ (\Delta T)_\pi}{K_{th}K_p\alpha_g} \qquad \ldots(14)$$

Inserting Eq. 13 (b) into Eq. 14 yields

$$(P_p)_\pi = \frac{K_{\sigma A}\lambda}{2K_{th}K_p\alpha_g(\partial n_{eff}/\partial T)\ L_w} \qquad \ldots(15)$$

Equation 15 indicates that π-phase shift pump power $(P_p)\pi$ is inversely proportional with both waveguide arm length Lw and thermo-optic coefficient the core material.

3. Results and Discussion

Ten COMSOL simulation tests were performed to evaluate the pump power required to generate a phase difference of π and to show how arm's length and core size affect the results. In the first five simulations, the core width is 0.23 μm, and the arm's length are 100, 200, 300, 400, and 500 μm, respectively. While in the last five simulations, the core width is 2.3 μm, and the arm's length were 100, 200, 300, 400, and 500 μm, respectively. As shown in Figs. 3, 4, and 5, one can note the strong confinement inside the core. Fig 3(a) and (b) show the signal confinement in the directional coupler DC for both core size 0.23 and 2.3 μm.

As a result of using graphene on the upper arm, one can observe that the signal intensity in the upper arm of MZI is less than the lower arm. This is because the pump is absorbed by graphene and changes the effective refractive index of upper arm to produce phase change, as shown in Figs. 4 (a) and (b). As shown in Figs. 5 (a), (b), and (c), the suggested switch can send the signal out of either Port 3 or Port 4, or both, at a rate that can be changed by changing the pumping power.

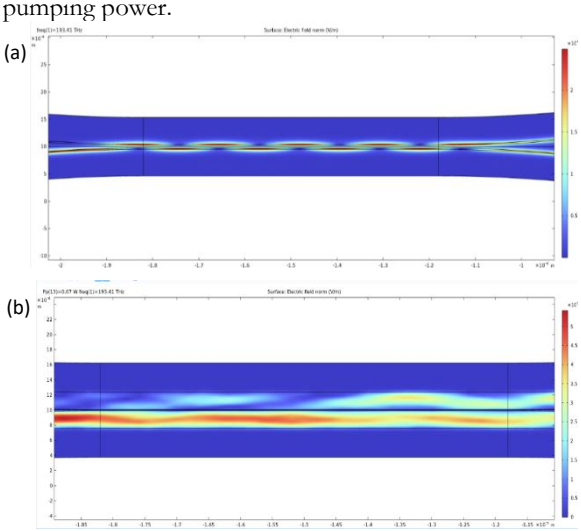

Figure (3): Signal confinement in DC (a) core width 0.23 μm, (b) core width 2.3 μm.

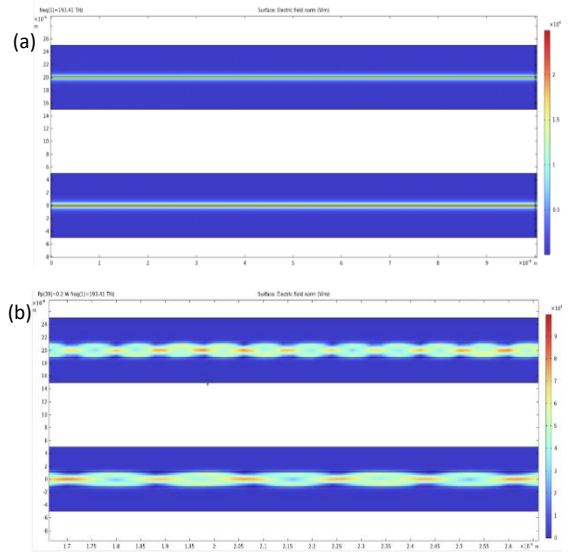

Figure (4): Signal confinement in both MZI arms (a) core width 0.23 μm, (b) core width 2.3 μm.

The power transmission, reflection, and absorption characteristics of the suggested all-optical switch are deduced as a function of pump power P_p using COMSOL simulation. The results are presented in Figs. 6-9 which correspond to a device designed with arm length Lw of 100, 200, 300, 400, and 500 μm, respectively. A 0.5 nm thickness of graphene layer is used to completely cover the upper arm of MZI (i.e., $l_g = L_w$). Each figure contains two parts (a) and (b), correspond to core width of 0.23 and 2.3 μm, respectively. Each part contains six curves corresponds to Reflection from Port, R11 = P_r/Pin, Transmission through Port2, T21, Transmission through Port3 (output 1), T31 = Pout1/Pin, Transmission through Port4 (output 2), T41 = Pout2/Pin, Total transmission, Pout1 + Pout2/Pin and absorption Power losses in the suggested device, P_{ab}.

Note that from power conversion law, the signal power components are related to the input signal power by

$$Pin = Pout1 + Pout2 + P_r + Pab \quad \ldots(16\ a)$$

equation 6.8a can rewritten as

$$Pin = T31 + T41 + R11 + R_L \quad \ldots(16\ b)$$

where R_L stand for relative loss (~Ploss/Pin).

Investigation the results in Figs. 6-9 reveals the following facts:

- The reflection from incident port (Port1) and the losses in the device are almost negligible. For example, R11 and R_L are 5.22×10^{-5} and 1.15×10^{-5}, respectively, when the device is designed with L_w = 100 μm and W_{co} = 0.23μm. these to be compared with R11 = 0.01058, and $R_L = 1.16\times10^{-6}$, when the core width increases to 2.3 μm.
- The peak output powers delivered from Port3 and Port4 are almost same. For example, the design with Lw = 100 μm and W_{co} = 0.23 μm yields T31 = 0.981 and T41 = 0.984. when W_{co} = 2.3 μm, T31 = 0.985 and T41 = 0.986.

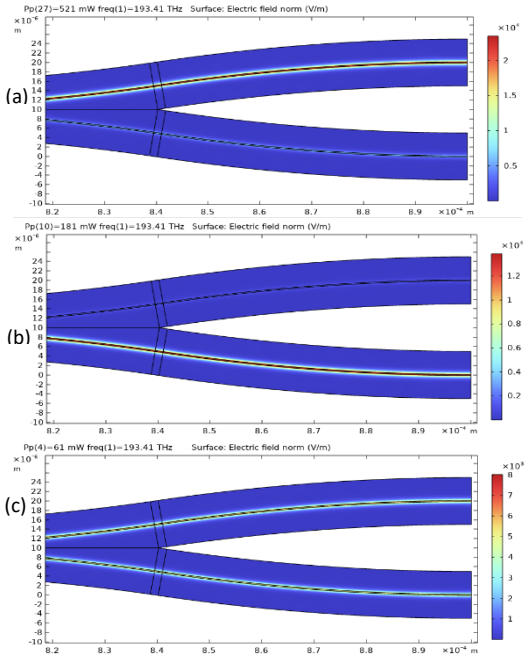

Figure (5): Signal confinement in both MZI output ports (a) power at Port 4, (b) power at Port 3, and (c) equal power at each port.

Figs. 6-9 can also be used as a guideline to estimate π-shift pump power $P_{p\pi}$ for different values of design structure parameters (arm length and core width). The values of $P_{p\pi}$ are estimated here as the value of ΔP_p that switch the state of the output ON and OFF (or vice versa). The results are listed in Table 6-1 and plotted in Fig. 6.1 as a function of arm length and for two values of core width, 0.23 μm, and 2.3 μm. table 6-1 also contains the ratio between π-shift pump power of 0.23 μm core width device, and 2.3 μm core width device ($R_{p\pi} = P_{p\pi}$ (0.23)/ $P_{p\pi}$ (2.3)). One can note that the π-shift pump power required is 50 mW for 300 μm arm length ($L_w = L_g$) which is 55.6 % compared to Ref. [1] with 288 μm graphene length (π-shift pump power 90 mW).

Table (1): π-shift pump power and the ratio between π-shift pump power of 0.23 μm core width device, and 2.3 μm core width device

Arm length (μm)	π-shift pump power (mW)		Ratio, Rpπ
	core width = 0.23 μm	core width = 2.3 μm	
100	270	160	0.59
200	120	80	0.57
300	100	50	0.5
400	60	40	0.67
500	55	35	0.64
600	50	30	0.60
700	45	25	0.56
800	40	20	0.50

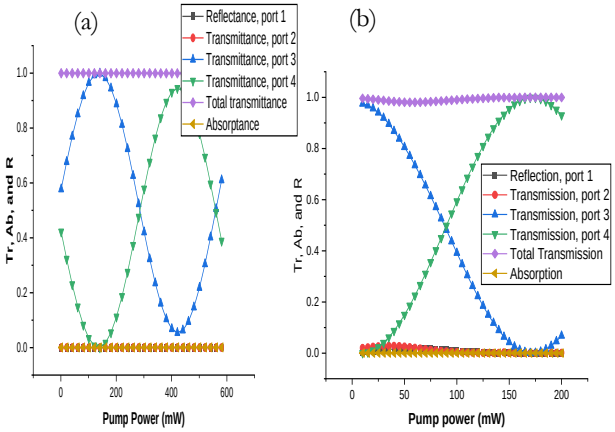

Figure (6): Transmission of Port2, Port3, Port4, reflection of signal by Port1, total transmission, and absorptance, for 100 μm arm's length (a) core width is 0.23 μm, and (b) core width is 2.3 μm.

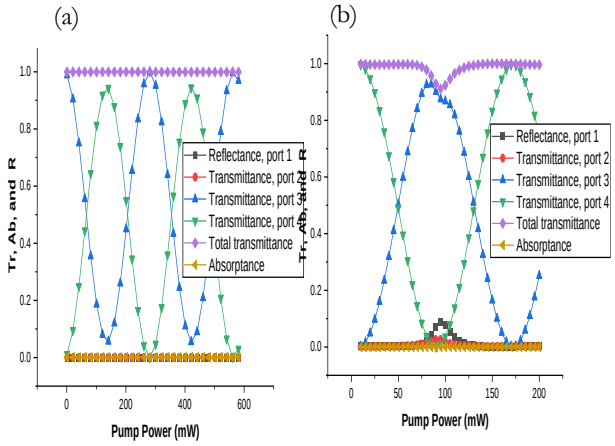

Figure (7): Transmission of Port2, Port3, Port4, reflection of signal by Port1, total transmission, and absorptance, for 200 μm arm's length (a) core width is 0.23 μm, and (b) core width is 2.3 μm.

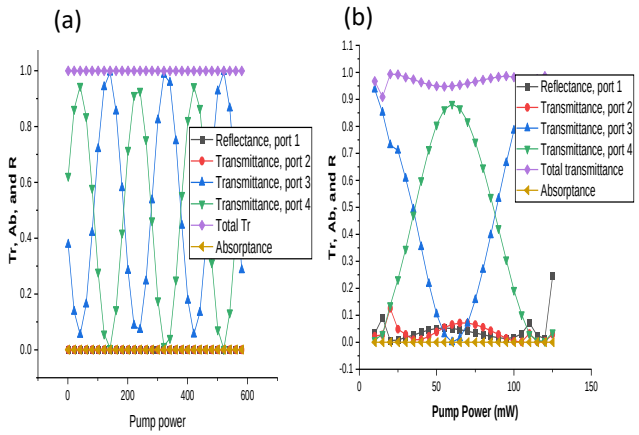

Figure (8): Transmission of Port2, Port3, Port4, reflection of signal by Port1, total transmission, and absorptance, for 300 μm arm's length (a) core width is 0.23 μm, and (b) core width is 2.3 μm

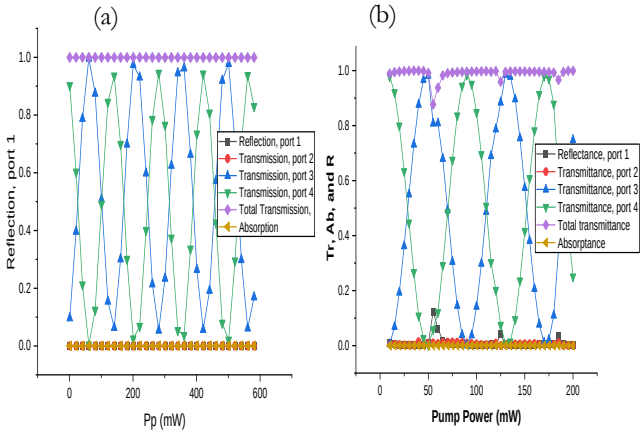

Figure (9): Transmission of Port2, Port3, Port4, reflection of signal by Port1, total transmission, and absorptance, for 400 μm arm's length (a) core width is 0.23 μm, and (b) core width is 2.3 μm.

The following two conclusions are drawn from the COMSOL simulation results presented in table 1 and Fig. 10

- The π-shift pump power $P_{p\pi}$ is almost inversely proportional to MZI arm length Lw and these results are accord with the developed mathematical model. For example, consider the device designed with core width = 0.23 μm and 100 μm arm length which has $P_{p\pi}$ =270 mW. When the device s redesigned with four- and eight-times arm length the value of $P_{p\pi}$ reduces to 0.22 and 0.15, respectively. These are too comparable with theoretical predictions of 1/4 = 0.25 and 1/8 = 0.125, respectively. For the 2.3 core width device, the corresponding reduction are 0.25 and 0.125. Note that the simulation results of the 0.23 μm core width device match that of theoretical model.
- The 2.3 μm core width device has $P_{p\pi}$ which is about 0.5-0.67 of the 0.23 μm core width counterpart.

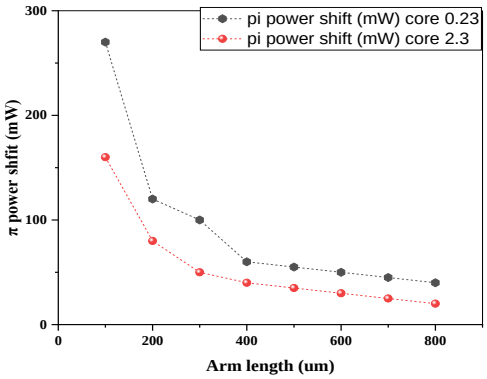

Figure (10): π- Shift power vs. MZI arm length.

On the other hand, both Δneff and T increase linearly with pump power (slop linear increment is 2.5×10^{-5} K^{-1}) as shown in Figs. 11 (a), (b) and (c) shows the variation of temperature T and the variation of the effective refractive index Δneff with the pumping power P_p. The dots and solid line in these figures correspond to COMSOL data and linear curve fitting,

respectively. Note that also effect by the size of core and the arm length, this happened because the size of the graphene changed. The larger the size of the graphene, the less pumping power it has.

Finally, the extinction ratio can be calculated as

$$(ER)_{bar} = 10\log_{10}\frac{P_{out1}}{P_{out2}} \quad \text{(dB)} \quad \ldots(17\text{ a})$$

$$(ER)_{cross} = 10\log_{10}\frac{P_{out1}}{P_{out2}} \quad \text{(dB)} \quad \ldots(17\text{ b})$$

For example, the bar-extinction Ratio a 100 μm arm length 0.23 μm and 2.3 μm core width, are 21.8 dB and 22.03 dB, respectively, and for 800 μm arm length 0.23 μm and 2.3 μm core width, are 25.2 dB and 17 dB, respectively. While, the cross-extinction Ratio a 100 μm arm length 0.23 μm and 2.3 μm core width, are 12.8 dB and 19.4 dB, respectively, and for 800 μm arm length 0.23 μm and 2.3 μm core width, are 13 dB and 19.9 dB, respectively.

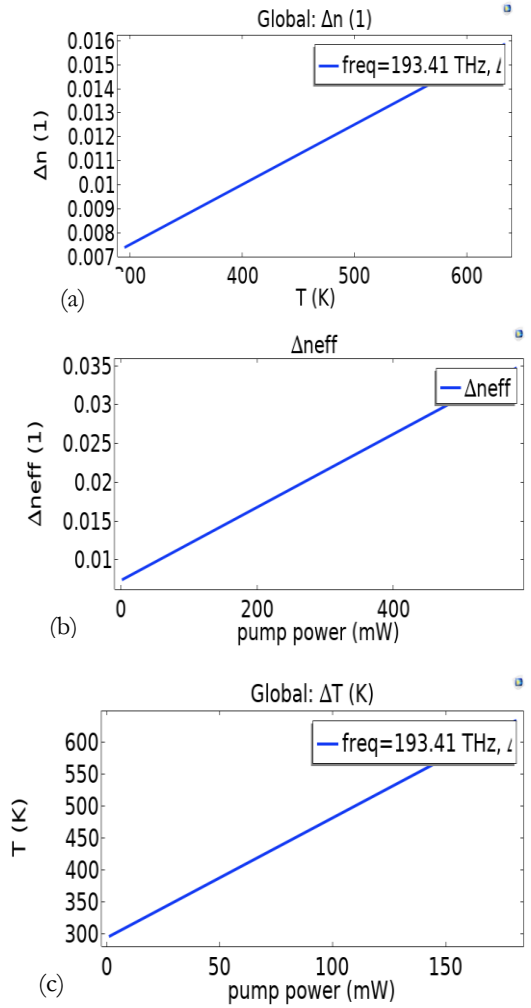

Figure (11): Variation of (a) temperature ΔT, and effective refractive index, (b) effective refractive index, and (c) temperature T with Pump Power P_p (Arm length 100 μm and width is 0.23 μm).

4. Conclusions

Using MZI rectangular waveguide configuration and buried graphene, this configuration leads to reduce the required switching pump power, moreover, during all-optical switching, these benefits make sure that both pump signal and probe light can work over a wide range of wavelengths. So, the suggested switch could be used in many all-optical signal processing applications on a single chip, such as all-optical switching, optical logic computing, photonic phase shifting, and many more.

5. References

[1] C. Qiu, C. Zhang, H. Zeng, and T. Guo, "High-performance graphene-on-silicon nitride all-optical switch based on a Mach–Zehnder interferometer," Journal of Lightwave Technology, vol. 39, no. 7, pp. 2099-2105, 2021.

[2] T. Hao, Z. Chang, and K. S. Chiang, "Externally pumped low-loss graphene-based fiber Mach-Zehnder all-optical switches with mW switching powers," Optics Express, vol. 27, no. 4, pp. 4216-4225, 2019/02/18, 2019.

[3] J. M. Lukens, H. H. Lu, B. Qi, P. Lougovski, A. M. Weiner, and B. P. Williams, "All-Optical Frequency Processor for Networking Applications," Journal of Lightwave Technology, vol. 38, no. 7, pp. 1678-1687, 2020.

[4] G. Roelkens, L. Liu, D. Liang, R. Jones, A. Fang, B. Koch, and J. Bowers, "III-V/silicon photonics for on-chip and intra-chip optical interconnects," Laser & Photonics Reviews, vol. 4, no. 6, pp. 751-779, 2010.

[5] I. Muhammad Aamir, M. Maria, S. Wajeehah, A. Waqas, A. A. M.-D. Kossi, and V. P. Phuong, "Plasmonic 2D Materials: Overview, Advancements, Future Prospects and Functional Applications," 21st Century Nanostructured Materials, V. P. Phuong, ed., p. Ch. 3, Rijeka: IntechOpen, 2021.

[6] J. S. Levy, A. Gondarenko, M. A. Foster, A. C. Turner-Foster, A. L. Gaeta, and M. Lipson, "Monolithically integrated multiple wavelength oscillator on silicon," arXiv preprint arXiv:0907.1077, 2009.

[7] A. Moscoso-Mártir, J. Müller, J. Hauck, N. Chimot, R. Setter, A. Badihi, D. E. Rasmussen, A. Garreau, M. Nielsen, E. Islamova, S. Romero-García, B. Shen, A. Sandomirsky, S. Rockman, C. Li, S. Sharif Azadeh, G.-Q. Lo, E. Mentovich, F. Merget, F. Lelarge, and J. Witzens, "Silicon Photonics Transmitter with SOA and Semiconductor Mode-Locked Laser," Scientific Reports, vol. 7, no. 1, pp. 13857, 2017/10/24, 2017.

[8] J. Joo, J. Park, and G. Kim, "Cost-effective 2× 2 Silicon Nitride Mach-Zehnder Interferometric (MZI) Thermo-optic Switch," IEEE Photonics Technology Letters, vol. PP, pp. 1-1, 03/12, 2018.

[9] K. Wu, Y. Wang, C. Qiu, and J. Chen, "Thermo-optic all-optical devices based on two-dimensional materials," Photonics Research, vol. 6, no. 10, pp. C22-C28, 2018.

[10] L. Gao, H. Ran, Y. Cao, Y. Li, W. Huang, L. Huang, D. Feng, X. Tang, and T. Zhu, "Coherent optical modulation of graphene based on coherent population oscillation," Optics Letters, vol. 44, no. 2, pp. 223-226, 2019.

[11] S. Yan, X. Zhu, L. H. Frandsen, S. Xiao, N. A. Mortensen, J. Dong, and Y. Ding, "Slow-light-

enhanced energy efficiency for graphene microheaters on silicon photonic crystal waveguides," Nature Communications, vol. 8, no. 1, pp. 14411, 2017/02/09, 2017.

[12] X. Gan, C. Zhao, Y. Wang, D. Mao, L. Fang, L. Han, and J. Zhao, "Graphene-assisted all-fiber phase shifter and switching," Optica, vol. 2, no. 5, pp. 468-471, 2015/05/20, 2015.

[13] R. Chu, C. Guan, Y. Bo, J. Liu, J. Shi, J. Yang, P. Ye, P. Li, J. Yang, and L. Yuan, "Graphene decorated twin-core fiber Michelson interferometer for all-optical phase shifter and switch," Optics Letters, vol. 45, no. 1, pp. 177-180, 2020/01/01, 2020.

[14] Y. Wang, F. Zhang, X. Tang, X. Chen, Y. Chen, W. Huang, Z. Liang, L. Wu, Y. Ge, Y. Song, J. Liu, D. Zhang, J. Li, and H. Zhang, "All-Optical Phosphorene Phase Modulator with Enhanced Stability Under Ambient Conditions," Laser & Photonics Reviews, vol. 12, no. 6, pp. 1800016, 2018.

[15] Y. Gao, G. Zhou, N. Zhao, H. K. Tsang, and C. Shu, "High-performance chemical vapor deposited graphene-on-silicon nitride waveguide photodetectors," Optics Letters, vol. 43, no. 6, pp. 1399-1402, 2018/03/15, 2018.

[16] H. Sun, Q. Qiao, Q. Guan, and G. Zhou, "Silicon Photonic Phase Shifters and Their Applications: A Review," Micromachines, vol. 13, no. 9, pp. 1509, 2022.

[17] R. Zhang, and W. Wang, "Perfect optical absorption in a single array of folded graphene ribbons," Optics Express, vol. 30, no. 25, pp. 44726-44740, 2022/12/05, 2022.

[18] Y. Yang, J. Lv, B. Lin, Y. Cao, Y. Yi, and D. Zhang, "Graphene-Assisted Polymer Waveguide Optically Controlled Switch Using First-Order Mode," Polymers, vol. 13, no. 13, pp. 2117, 2021.

[19] N. Ali, M. F. Abdullah, and R. Kumar, "Silicon photonic switches," Optical Switching: Device Technology and Applications in Networks, pp. 239-255, 2022.